A Hybrid System for Myocardial Infarction Classification with Derived Vectorcardiography

Yu-Hung Chuang, Ching-Yu Lee, Yin-Husan Chen, and Wen-Whei Chang

Institute of Electrical and Computer Engineering, National Yang Ming Chiao Tung University, Hsinchu, Taiwan
E-mail: wwchang@nycu.edu.tw

***Abstract*—The 12-lead electrocardiography (ECG) remains the most rapid and widely used diagnostic test for patients with myocardial infarction (MI). Most wearable ECG devices only provide single limb-lead measurement, limiting their practical applicability for MI diagnosis. The ability to transform from single-lead ECG to 3-lead vectorcardiography (VCG) enables wider use of wearable devices in clinical diagnostics. This study presents a patient-specific transformation for VCG synthesis using temporal convolutional networks in variational mode decomposition domain. MI-induced changes in morphological and temporal wave features are extracted from the derived VCG via spline curve approximation. After feature extraction, a multilayer perceptron classifier is used to classify different types of MI. Experiments on the PTB diagnostic database show that the proposed system achieves satisfactory performance in differentiating MI patients from healthy subjects and localizing infarcted area.**

***Keywords*— myocardial infarction, vectorcardiography, temporal convolutional network, spline curve fitting, variational mode decomposition**

I. Introduction

Myocardial infarctions (MI) is one of the leading causes of mortality worldwide. It results from an occlusion of the coronary artery and insufficient blood supply to the myocardium. MI can be further classified into various types depending on the localization of infarcted area. In clinical setting, MI is diagnosed using 12-lead electrocardiography (ECG) [1] as well as 3-lead vectorcardiography (VCG) [2]. The standard 12-lead ECG consists of three limb leads (I, II, III), three augmented limb leads (aVR, aVL, aVF) and six chest leads (V_1 to V_6). According to electrode positioning, the 12 ECG leads can be used to localize different types of MI, such as inferior leads (II, III, aVF), septal leads (V_1, V_2), anterior leads (V_3, V_4), and lateral leads (I, aVL, V_5, V_6). A typical waveform of ECG beat consists of a P wave, a QRS-complex, and a T wave. ECG signs suggestive of MI include ST-segment deviation or changes in the shapes of Q-wave and T-wave, using which physicians can localize infarcted areas. However, it may be noted that 12-lead ECG requires ten electrodes for recording and some of the leads contain redundant information. Instead, three Frank leads (V_x, V_y, V_z) scanned in three orthogonal planes of the body are used for VCG measurements. Moreover, previous studies [3] have demonstrated that VCG provides a higher sensitivity for diagnosis of MI as well as ischemic heart diseases. Thus in this study, VCG signal is processed to extract clinically significant features that will allow for MI classification.

Most patients suffer from MI without awareness, and their recovery depends critically on early diagnosis and timely treatment. In recent years, a number of computer-aided diagnostic approaches have been proposed for MI detection and localization [4–10]. Most of these approaches extract clinically significant features from multi-lead ECG signals and apply machine learning-based classifiers in the classification stage. Various informative features have been extracted to represent the ECG beats, such as morphological features [4] as well as frequency and wavelet-based features [5,6]. Alternatively, some studies have attempted to identify abnormalities in the VCG morphology such as the QRS and T-wave loops [10]. Generally, the prerequisite is to identify characteristic waves of ECG beats before performing feature extraction. Although various methods have been proposed for ECG wave delineation [11], they still have some limitations for characterization of MI beats. Recognizing this, we apply spline curve fitting [12] to the entire heartbeat and use fitted coefficients as VCG representing features. Its advantage is that all of the characteristic waves can be included in the spline approximation so that poor quality features resulting from delineation errors can be avoided. Moreover, the spline's flexibility in approximating curves with different degrees of smoothness at different locations is ideal for representing the semi-periodic VCG signal.

Another problem which requires further investigation is to test the feasibility of wearable devices in MI classification. Most wearable devices provide insufficient information due to limitations in the number of leads and measurement positions. Incorporating the derived VCG techniques can help monitor the three-dimensional electrical activities of human hearts. A common assumption in previous works [13,14] is that the heart-torso electrical system is linear and quasi-static, allowing for the use of linear transformation to derive the VCG from reduced-lead set of the 12-lead ECG. These transforms can be either patient-specific or generic, with the former being learned from a single patient's data and the latter requiring data from a group of patients. Atoui et al. [15] used a nonlinear transformation for deriving the VCG based on artificial neural networks. A weakness for these approaches is that they focused on spatially correlated information in different leads, with less emphasis placed upon temporal correlation between different waves within a single lead. Moreover, all of these methods require at least two synchronously acquired leads, hampering their applicability to the present context. Since lead I ECG is provided by most wearable devices, we propose a derived VCG system by considering the lead I ECG as input and

Frank XYX leads as output of the system. Our approach uses temporal convolutional network (TCN) [16] to exploit both intra- and inter-lead correlations of ECG signals. The TCN offers the benefit of having a more flexible receptive field and a better learning ability to model long-term temporal dependencies in time series data. Also, due to the parallelizable architecture of TCN, the training time compared to recurrent neural networks like long short-term memory (LSTM) [17] is significantly reduced. Considering that ECG are non-stationary, lead I signal is decomposed into different intrinsic mode functions by variational mode decomposition (VMD) [18]. The advantage is that VMD is robust against noise and helps TCN learn the ECG morphology from different characteristic waves.

II. PROPOSED METHOD

This study proposes a new method for MI classification using the single-lead derived VCG. As shown in Fig. 1, the proposed method consists of four stages, i.e., VMD, VCG synthesis, feature extraction, and MI classification. The raw ECG signals are preprocessed to remove various kinds of noise associated with them. Next, a patient-specific lead reconstruction method is used to synthesize the 3-lead VCG from lead-I ECG. In the feature extraction stage, clinically significant features are extracted from derived Frank XYZ leads that quantify the VCG abnormalities due to MI. Later in the classification stage, the most likely ECG class is predicted from the analysis of the feature data.

Fig. 1 Block diagram of the proposed MI classification system.

A. Dataset and Data Preprocessing

Measured ECG of various morphologies were taken from PTB diagnostic database [19]. This database has 549 ECG records from 290 subjects and each record contains 12-lead ECG and 3-lead VCG. From the database, a total of 26080 heartbeats from 52 healthy subjects and 143 MI patients were included in the analysis. ECG beats were further divided into 12 classes: anterior (AMI), anterior-lateral (ALMI), anterior-septal (ASMI), anterior-septal-lateral (ASLMI), inferior (IMI), inferior-lateral (ILMI), inferior-posterior (IPMI), inferior-posterior-lateral (IPLMI), lateral (LMI), posterior (PMI), posterior-lateral (PLMI), and healthy control (HC). The raw ECG signal is typically contaminated by high-frequency noise as well as baseline wander. To remove these artifacts for ECG enhancement, we down-sampled the raw ECG signal to 500 Hz and then filtered the signal using a 0.5-150 Hz band-pass filter.

B. Variational Mode Decomposition

The purpose of VMD [18] is to decompose lead I ECG signal into a series of band-limited modes. It is assumed that each mode u_k is concentrated around its center frequency ω_k. The bandwidth of each mode is estimated in three steps. First, the associated analytic signal is computed by the Hilbert transform to obtain a unilateral frequency spectrum. Then, the spectrum is shifted to its baseband by mixing with an exponential tuned to the estimated center frequency. Finally, the H^1 Gaussian smoothness of the demodulated signal is used to determine the bandwidth of each mode. The resulting constrained variational problem is given by

$$\min_{\{u_k\},\{\omega_k\}} \left\{ \sum_{k=1}^{K} \left\| \partial_t \left[\left(\delta(t) + \frac{j}{\pi t} \right) * u_k(t) \right] e^{-j\omega_k t} \right\|_2^2 \right\} \; s.t. \sum_{k=1}^{K} u_k(t) = f(t) \quad (1)$$

where $f(t)$ is the lead I signal to be decomposed, K is the number of modes, $\delta(t)$ is the Dirac distribution, and $*$ denotes the convolution. To convert the problem (1) into an unconstrained optimization problem, the augmented Lagrangian function can be defined as follows:

$$\Gamma(\{u_k\},\{\omega_k\},\lambda) = \alpha \sum_{k=1}^{K} \left\| \partial_t \left[\left(\delta(t) + \frac{j}{\pi t} \right) * u_k(t) \right] e^{-j\omega_k t} \right\|_2^2 + \left\| \sum_{k=1}^{K} u_k(t) - f(t) \right\|_2^2 + \langle \lambda(t), f(t) - \sum_{k=1}^{K} u_k(t) \rangle \quad (2)$$

where λ is the Lagrangian multiplier and α is the penalty factor. The alternate direction method of multipliers [20] is applied to find the saddle point of augmented Lagrangian.

The VMD algorithm has been implemented using the wavelet toolbox in MATLAB. The VMD parameters, which may influence the decomposition results, are the number of modes (K), the penalty factor (α), the convergence tolerance (ϵ), the time-step of the dual ascent (τ) and method to initialize center frequencies ($init$). In this study, VMD parameters except K are initialized with default values as follows: $\tau = 0.01$, $init = 1$, $\alpha = 1000$, $\epsilon = 5e-6$. We empirically chose $K = 4$ as the number of modes, because that ECG energy is mostly concentrated in the first to the fourth modes, which correspond respectively to the major characteristic waves of ECG beats.

C. VCG Synthesis

After signal decomposition, we apply a VCG synthesizer which can be viewed as a cascade of two stages. In the first stage, TCNs were employed to learn the decomposed modes and in the second stage, the TCN outputs are merged into the final synthesis through a fully connected layer. The architecture of the proposed system is shown in Fig. 2. The system starts by applying a sliding window which spreads an L-length segment of decomposed data across the input neurons of TCN. TCNs are employed for lead synthesis and their outputs from four decomposed modes are concatenated and fed to a fully-connected layer to obtain the derived VCG. At the model estimation stage, the synthesizer was trained for each individual using four decomposed data series of lead-I ECG as input and three Frank leads as output of the model. Let $u_k(t)$ denote the k-th VMD mode at time t and let $V_x(t), V_y(t), V_z(t)$ denote Frank XYZ lead data at time t. For an L-length window, suppose the pair (U_t, Y_t) contain the data $U_t = \{(u_k(t-L+1), \dots, u_k(t)), k = 1,2,3,4\}$ and its corresponding output $Y_t = \{V_x(t), V_y(t), V_z(t)\}$. Given a training data set $\{(U_t, Y_t), t = 1,2 \dots, T\}$, the smooth mean absolute error between measured and reconstructed VCG is minimized through supervised learning.

The main building blocks of TCN [16] are causal convolution, dilated convolution, and residual blocks. The

convolutions of TCN are causal, where a subsequent output at time t is computed only with the region no later than time t in the previous layer. Simple causal convolutions have the disadvantage to only look back at history with size linear in the depth of the network. Considering that ECG signals generally have long historical information, using causal convolution may lead to very deep networks, which are not conducive to network training. This issue can be addressed by dilated convolution, in which the filter is applied across a region greater than its size by skipping input data at regular intervals. In this study, we use an exponential dilation factor $d = 2^i$ for level i in the network. This effectively allows the network to have a large receptive field and to capture long-term temporal dependencies in the input sequence. If the input sequence is too long, however, the network will be inevitably deep and faced with the risk of vanishing gradient, exploding gradient and networking degradation. To resolve the problem, residual blocks have been shown effective in learning deep networks. Within a residual block, residual connections are used to prevent networking degradation, while weight normalization and rectified linear unit (ReLU) activation function are used to solve gradient disappearance and explosion. For the TCN architecture, we used the implementation from the GitHub repository provided by Bai et al. [16]. We empirically chose a level-6 network with a filter size of 7 and 30 neurons in each hidden layer. The TCN is trained with the Adam optimizer, a mini-batch size of 128 and a learning rate of 0.002.

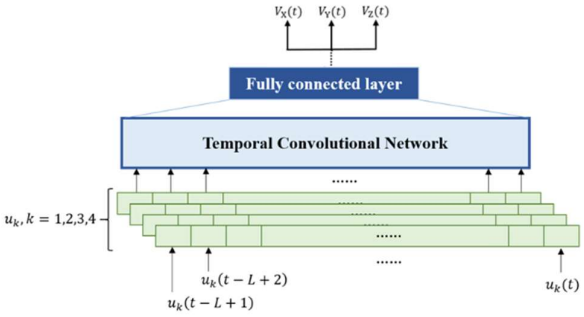

Fig. 2 TCN-based synthesizer with a sliding window approach.

D. Feature Extraction

MI classification is essentially a pattern recognition problem consisting of two stages: feature extraction and classification. In the feature extraction stage, Frank XYZ leads of the derived VCG are individually processed in the following steps. First, we detect the R peak in each QRS complex using the Pan-Tompkins algorithm [21] and split the lead signal into heartbeat segments between two neighboring R peaks. Since the heartbeats may have different lengths, each heartbeat is period normalized to a fixed length of 400 samples via cubic spline interpolation. This choice was based on the observation that the average heartbeat length is about 0.8 sec, corresponding to 400 samples for a sampling frequency of 500 Hz. In order to make different lead signals comparable to each other, the min-max normalization was applied to scale both the amplitude and time in the range of [0,1]. For the k-th heartbeat with length N_k, let $\alpha_k = N_k/400$ denote the time scaling factor and let $\beta_k^{(1)}, \beta_k^{(2)}, \beta_k^{(3)}$ denote the amplitude scaling factor of Frank X, Y, Z lead, respectively. Once the heartbeats have been segmented and normalized, spline curve fitting [12] is applied to the entire heartbeat to model all of the characteristic waves and fitted coefficients are used as VCG representing features.

Splines are piecewise polynomial approximations of a signal defined by constraint points on each piecewise segment known as knots. Since VCG signal has numerous clinically-relevant turning points, the spline represented as a linear combination of p-degree B-spline basis function has been chosen as the approximation function. The knot vector $\{\zeta_j\}_0^m = \{\zeta_j, 0 \le j \le m\}$ is a non-decreasing sequence, where the first $(p+1)$ knots are all equal to 0.0025 and the last $(p+1)$ knots are all equal to 1. The knots from ζ_{p+1} to ζ_{m-p-1} correspond to interior knots which are generated via the knot averages as follows:

$$\zeta_k = \frac{\tau_{k+1} + \tau_{k+2} + \cdots + \tau_{k+p}}{p}, p+1 \le k \le m-p-1 \quad (6)$$

where $\{\tau_{p+1}, \tau_{p+2}, \ldots, \tau_m\}$ is an arithmetic sequence with the first term $\tau_{p+1} = 0.0025$ and the last term $\tau_m = 1$. The spline curve approximation can be expressed as follows:

$$\mathrm{s(t)} = \sum_{i=0}^{n} a_i B_{i,p}(t) \quad (7)$$

where $\mathrm{n = m - p - 1}$ and a_i represents the i-th B-spline coefficient. $B_{i,p}(t)$ denotes the i-th p-degree B-spline basis function which is computed recursively [12] as follows:

$$B_{i,0}(t) = \begin{cases} 1, & \zeta_i \le t \le \zeta_{i+1} \\ 0, & otherwise \end{cases} \quad (8)$$

$$B_{i,j}(t) = \frac{t - \zeta_i}{\zeta_{i+j} - \zeta_i} B_{i,j-1}(t) + \frac{\zeta_{i+j+1} - t}{\zeta_{i+j+1} - \zeta_i} B_{i+1,j-1}(t) \quad (9)$$

The vector of coefficients $\{\mathrm{a}_i, 0 \le i \le n\}$ is calculated by using the least square spline approximation. It was empirically determined that $n = 15$ gives a good trade-off between computational efficiency and the quality of fit. Each normalized heartbeat is transformed into 16 features $\{\mathrm{a}_0, \mathrm{a}_1, \ldots, \mathrm{a}_{15}\}$, and three Frank leads during the time of a given heartbeat have 48 features. Together with time scaling factor α_k and amplitude scaling factors $\{\beta_k^{(1)}, \beta_k^{(2)}, \beta_k^{(3)}\}$, the complete heartbeat of derived 3-lead VCG is transformed as a 52-dimensional feature vector.

E. MI Classification

After feature extraction, a multilayer perceptron (MLP) classifier is used for classification into 12 classes of ECG beats. The attractiveness of MLPs comes from their information processing characteristics such as nonlinearity,

high parallelism, learning and generalization capabilities [22]. An MLP is a network composed of parallel layers of neurons. In building MI classifiers, the input layer receives spline-fitted features from the derived VCG, and the output layer provides the predicted ECG class. The relations between the input and output layers are expressed through the weights and biases of hidden layers. All of the weights were initialized to small random numbers and then subjected to incremental changes by the error backpropagation algorithm based on the cross-entropy loss function. For classification purposes, we employ the one-hot encoding scheme to represent the MLP outputs as binary vectors, each vector consists of 0s in all cells with the exception of a single 1 in an entry corresponding to the most likely ECG class. A series of experiments were performed to optimize the MLP topologies used for MI classification. Based on the results, we chose the MLP topology with 52 input nodes (one for each spline-fitted feature), 12 output nodes (one for each ECG class) and two hidden layers which have 300 and 275 nodes, respectively. With respect to the activation function, ReLU is used for the hidden layer and softmax function for the output layer.

III. Results and Discussion

Computer simulations were conducted to evaluate the validity of the proposed method for MI classification. ECG records from the PTB diagnostic database [19] were chosen to represent a wide variety of diagnostic classes. ECG records from 52 HC subjects are denoted as dataset DS1, and ECG records from 143 MI patients are denoted as dataset DS2. A preliminary experiment was first conducted to examine the performance dependence of VCG synthesis on the sliding window size L of TCN models. Based on the results, we empirically chose $L = 250$ in the sequel. We next compare the reconstruction performance of using LSTM [17], TCN and VMD-TCN for learning the derived VCG models. For comparison purposes, the LSTM consists of 250 input nodes, three output nodes, six hidden layers with each containing 30 neurons. The RMSE performances of VCG synthesis by five-fold cross-validation are shown in Table 1. Simulation results indicate that the TCN is preferred to LSTM for use in constructing the lead synthesizer because the TCN can better exploit long-term temporal dependencies. In addition, as compared to LSTM, TCN's training time is greatly reduced due to its parallelizable architecture. Overall, the TCN synthesizer yielded an average RMSE of 10.38 and 14.10 for dataset DS1 and DS2, respectively, implying that MI subject data were less accurately reconstructed than HC subjects. Further analysis indicated that the VMD-TCN synthesizer achieved the best performance for all test samples. Specifically, the VMD-TCN synthesizer reduces the average RMSE to 9.22 and 12.75 for dataset DS1 and DS2, respectively. To elaborate further, visual inspection of the reconstructed VCG signals was carried out by an experienced physician who was blinded to the experimental setting. The derived VCG was shown to be comparable to measured VCG in terms of identifying various cardiac abnormalities. To illustrate this, Fig. 3 compares the measured and reconstructed Frank XYZ leads for an MI patient.

TABLE 1.
RMSE BETWEEN MEASURED AND DERIVED FRANK LEADS USING VARIOUS MODELS.

Model	Dataset	$\hat{V}_X$	$\hat{V}_Y$	$\hat{V}_Z$	Mean
LSTM	DS1	10.7844	12.7513	9.8004	11.1120
	DS2	16.7724	21.3066	17.2442	18.4411
TCN	DS1	9.54371	12.2234	9.3744	10.3805
	DS2	11.9165	17.4396	12.9563	14.1042
VMD-TCN	DS1	8.6680	10.8579	8.12416	9.21671
	DS2	10.9615	15.7614	11.5133	12.7454

The next step is to assess the performance of MLP classifiers for classification of normal and 11 MI classes. One problem with the PTB diagnostic database is the high imbalance between the number of heartbeats belonging to each ECG class. Training an MLP classifier with unbalanced data usually leads to a certain bias towards the majority class. Recognizing this, we applied the Synthetic Minority Over-sampling Technique (SMOTE) [23] before starting the training process. The performance analysis is based on the accuracy (ACC), sensitivity (SEN), and specificity (SPE) represented in the form of confusion matrix. For a given class, accuracy is the proportion of correctly classified samples to the total number of samples. Sensitivity and specificity are defined as the proportion of positives and negatives that are correctly identified, respectively. Table 2 presents the 5-fold cross-validation test results using various lead configurations. Simulation results indicated that using lead I ECG yielded an overall accuracy of 48.94%, suggesting that it cannot provide sufficient cues for reliable classification. To elaborate further, we show in Table 3 the confusion matrix of all the 12 classes for lead I ECG beats. It was found that the notably low classification accuracy can be attributed to the high confusions made across anterior MI group (AMI, ALMI, ASMI, ASLMI) and inferior MI group (IMI, ILMI, IPMI, IPLMI). For instance, 14.19% of the ECG beats notated in ASMI were classified as representing IMI and 13.10% of the IMI beats were classified as being ASMI. Further analysis shows that combining multiple derived Frank leads yields substantial improvement over measured lead I for all test samples. Overall, using derived Frank XYZ leads achieved the best performance with an accuracy of 99.72%, compared with 47.38% for $\hat{V}_x$ and 93.13% for $\hat{V}_x + \hat{V}_y$. Table 4 shows the confusion matrix of all classes obtained using MLP classifier on the derived Frank XYZ leads. A comparison between Tables 3 and 4 indicates that the improvement can be seen in the following areas. First, the derived VCG can reduce a significant portion of confusions across anterior

and inferior MI groups. For instance, only 0.12% of ECG beats notated in ASMI were misclassified as representing IMI, the corresponding value for lead I being 14.19%. Second, the derived VCG significantly increased the sensitivity of healthy subjects to 99.90%, compared with 57.50% for lead I.

Table 5 summarizes the studies employing different techniques in MI classification with the same PTB database. The numbers of ECG leads and MI classes are important factors correlated with diagnosis efficiency, and should be noted when comparing their relative performances. Arif et al. [4] used 12-lead ECG and time domain features such as T-wave amplitude, Q-wave and ST-level elevation, reporting overall accuracy of 98.8% on 11 ECG classes. Noorian et al. [5] used neural network classifiers and wavelet coefficients as features extracted from 12-lead ECG. Acharya et al. [6] evaluated 11 ECG classes with nonlinear features based on wavelet transform by only using lead V_3 ECG signal.

TABLE 2.
CLASSIFICATION RESULTS WITH VARIOUS LEAD CONFIGURATIONS.

Leads	ACC(%)	SEN(%)	SPE(%)
$\boldsymbol{I}$	48.94%	67.36%	95.05%
$\hat{\boldsymbol{V}}_x$	47.38%	58.10%	95.02%
$\hat{\boldsymbol{V}}_x + \hat{\boldsymbol{V}}_y$	93.13%	95.52%	99.32%
$\hat{\boldsymbol{V}}_x + \hat{\boldsymbol{V}}_y + \hat{\boldsymbol{V}}_z$	99.72%	99.70%	99.97%

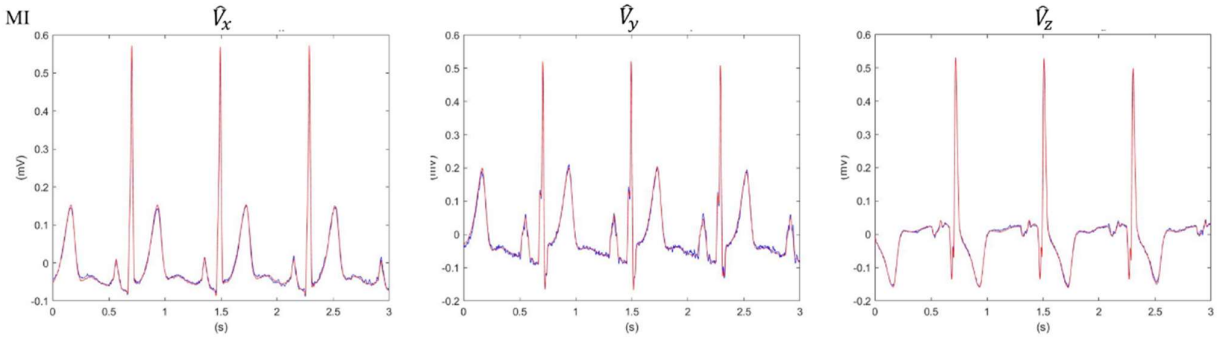

Fig. 3. Comparison between the measured (blue) and derived (red) Franks leads for an MI patient.

TABLE 3. CONFUSION MATRIX FOR MI CLASSIFICATION USING MEASURED LEAD I ECG.

	Predicted															
Notated	**AMI**	**ALMI**	**ASMI**	**ASLMI**	**IMI**	**ILMI**	**IPMI**	**IPLMI**	**LMI**	**PMI**	**PLMI**	**HC**	**Total**	**ACC**	**SEN**	**SPE**
AMI	1434	186	146	1	215	312	16	73	64	6	34	257	2744	91.21	52.26	95.89
ALMI	107	1295	297	16	176	107	54	47	7	133	111	142	2492	91.54	51.97	95.81
ASMI	190	298	1597	16	573	611	44	129	105	3	110	361	4037	84.37	39.56	92.76
ASLMI	0	0	0	132	0	0	0	0	0	0	0	0	132	99.62	100	99.62
IMI	265	233	587	46	1242	503	113	108	58	48	272	1005	4480	79.68	27.72	90.70
ILMI	158	73	80	0	283	1714	6	253	125	2	3	392	3089	84.90	55.49	88.94
IPMI	5	10	1	0	2	1	307	0	0	0	0	2	328	98.93	93.60	99.00
IPLMI	25	60	97	1	114	176	2	416	19	0	12	120	1042	93.70	39.92	95.98
LMI	0	0	1	0	0	2	0	0	153	0	0	0	156	98.20	98.08	98.20
PMI	0	0	0	0	0	0	0	0	0	135	0	0	135	99.14	100	99.13
PLMI	0	0	5	0	2	2	0	2	0	0	261	11	283	96.62	92.23	96.67
HC	190	109	347	17	599	776	18	375	79	29	301	3842	6682	79.96	57.50	87.90

TABLE 4. CONFUSION MATRIX FOR MI CLASSIFICATION USING DERIVED FRANK XYZ LEADS.

	Predicted															
Notated	**AMI**	**ALMI**	**ASMI**	**ASLMI**	**IMI**	**ILMI**	**IPMI**	**IPLMI**	**LMI**	**PMI**	**PLMI**	**HC**	**Total**	**ACC**	**SEN**	**SPE**
AMI	2735	2	2	0	1	1	0	1	0	0	0	2	2744	99.93	99.67	99.96
ALMI	4	2479	2	0	6	0	0	0	0	0	0	1	2492	99.92	99.48	99.97
ASMI	4	1	4023	0	5	1	0	0	0	0	0	3	4037	99.91	99.65	99.96
ASLMI	0	0	0	132	0	0	0	0	0	0	0	0	132	100	100	100
IMI	2	1	2	0	4467	2	2	1	0	1	0	2	4480	99.88	99.71	99.92
ILMI	0	2	1	0	1	3082	0	1	0	0	0	2	3089	99.95	99.77	99.97
IPMI	0	1	0	0	0	1	325	1	0	0	0	0	328	99.98	99.09	99.99
IPLMI	0	0	1	0	1	2	1	1036	0	0	0	1	1042	99.95	99.42	99.97
LMI	0	0	0	0	0	0	0	0	156	0	0	0	156	100	100	100
PMI	0	0	0	0	0	0	0	0	0	135	0	0	135	100	100	100
PLMI	0	0	0	0	0	0	0	1	0	0	282	0	283	100	99.65	100
HC	0	1	1	0	3	0	0	2	0	0	0	6675	6682	99.93	99.9	99.94

Another strategy can be seen in [7–9], where end-to-end methods based on convolutional neural networks were used for MI classification. Towards addressing the challenges in wearable device scenarios, our work, as well as earlier studies [6,7], was focused on single-lead rather than 12-lead exploration. Our results are generally better than those of MI classifiers in the literature. Overall, the proposed method obtained an accuracy of 99.72%, sensitivity of 99.70% and specificity of 99.97%. With this performance, our proposed model has the potential to provide an early and accurate diagnosis of MI in wearable ECG devices.

TABLE 5.
COMPARISON OF THIS STUDY WITH OTHER STUDIES USING THE PTB DIAGNOSTIC DATABASE.

Ref	Leads	No. of classes	ACC(%)	SEN(%)	SPE(%)
[4]	12 leads	11	98.80%	98.67%	98.71%
[5]	12 leads	10	95.36%	99.09%	94.23%
[6]	V_3	11	98.74%	99.55%	99.16%
[7]	I	4	95.25%	92.40%	97.70%
[8]	12 leads	11	99.78%	99.84%	99.98%
[9]	12 leads	6	99.11%	99.02%	99.10%
Proposed method	I	12	99.72%	99.70%	99.97%

IV. CONCLUSIONS

This study focuses on two issues: synthesis of 3-lead VCG and extraction of VCG features, to develop an MI classifier that is suitable for wearable devices with only a single lead recording. We first emphasized the importance of exploiting both intra- and inter-lead correlations for learning the derived VCG models. This task was accomplished by using a patient-specific transformation based on TCN in the VMD domain. Performance is further enhanced by using spline curve approximation to extract clinically significant features from the derived VCG. After the feature extraction, an MLP classifier is used for classification of normal and 11 types of ECG beats. Experiments on the PTB diagnostic database demonstrate the validity of the proposed MI classification system with an accuracy of 99.72%, sensitivity of 99.70%, and specificity of 99.97%.

ACKNOWLEDGMENT

This work was supported by the Ministry of Science and Technology, Taiwan, under Grant MOST 111-2221-E-A49-075. The authors are gratefully to Dr. Chein-Fang Chiu for her help in proving comprehensive medical consultation.

REFERENCES

[1] Plonsey, J.M. 12-lead ECG system. Bioelectromagnetism 1995, 15, 23–34.
[2] Frank, E. An accurate clinically practical system for spatial vectorcardiography. Circulation 1956, 13, 737–749.
[3] Panagiotou, C.; Dima, S.-M.; Mazomenos, E.B.; Rosengarten, J.; Maharatna, K.; Gialelis, J.; Morgan, J. Detection of myocardial scar from the vcg using a supervised learning approach. Annu. Int. Conf. IEEE Eng. Med. Biol. Soc. 2013, 7326–7329.
[4] Arif, M.; Malagore, I.A.; Afsar, F.A. Detection and localization of myocardial infarction using K-nearest neighbor classifier. J. Med. Syst., vol. 36, pp. 279-289, 2012.
[5] Noorian, A.; Dabanloo, N.J.; Parvanch, S. Wavelet based method for localization of myocardial infarction using the electrocardiogram. Proc. Comput. Cardiol. 2014, 2014, 645–648.
[6] Acharya, U.R.; Fujita, H.; Sudarshan, V.K.; Oh, S.L.; Adam, M.; Koh, J.E.W.; Tan, J.H.; Ghista, D.N.; Martis, R.J.; Chua, C.K.; et al. Automated detection and localization of myocardial infarction using electrocardiogram: A comparative study of different leads. Knowl. Based Syst. 2016, 99, 146–156.
[7] Lui, H.W.; Chow, K.L. Multiclass classification of myocardial infarction with convolutional and recurrent neural networks for portable ECG devices. Informat. Med. Unlocked 2018, 13, 26–33.
[8] Baloglu, U.B.; Talo, M.; Yildirim, O.; Tan, R.S.; Acharya, U.R. Classification of myocardial infarction with multi-lead ECG signals and deep CNN. Pattern Recognit. Lett. 2019, 122, 23–30.
[9] Fu, L.; Lu, B.; Nie, B.; Peng, Z.; Liu, H.; Pi, X. Hybrid network with attention mechanism for detection and location of myocardial infarction based on 12-lead electrocardiogram signals. Sensors 2020, 20, 1020.
[10] Aranda, A.; Bonizzi, P.; Karel, J.; Peeters, R. Performance of Dower's inverse transform and Frank lead system for identification of myocardial infarction. Annu. Int. Conf. IEEE Eng. Med. Biol. Soc. 2015, 4495–4498.
[11] Banerjee, S.; Gupta, R.; Mitra, M. Delineation of ECG characteristic features using multiresolution wavelet analysis method. Measurement 2012, 45, 474–487.
[12] Dung, V.T.; Tjahjowidodo, T. A direct method to solve optimal knots of B-spline curves: An application for non-uniform B-spline curves fitting. PLoS ONE 2017, 12.
[13] Edenbrandt, L.; Pahlm, O. Vectorcardiogram synthesized from 12-lead ECG: Superiority of the inverse Dower matrix. J. Electrocardiol. 1988, 21, 361–367.
[14] Dawson, D.; Yang, H.; Malshe, M.; Bukkapatnam, S.T.S.; Benjamin, B.; Komanduri, R. Linear affine transformations between 3-lead (Frank XYZ leads) vectorcardiogram and 12-lead electrocardiogram signals. J. Electrocardiol. 2009, 42, 622–630.
[15] Atoui, H.; Fayn, J.; Rubel, P. A novel neural-network model for deriving standard 12-lead ECGs from serial three-lead ECGs: Application to self-care. IEEE Trans. Inf. Technol. Biomed. 2010, 14, 883–890.
[16] Bai, S.; Kolter, J.Z.; Koltun, V. An empirical evaluation of generic convolutional and recurrent networks for sequence modeling. arXiv:1803.01271, 2018.
[17] Hochreiter S.; Schmidhuber J. Long Short-Term Memory. Neural Comput. 1997, 9, 1735–1780.
[18] Dragomiretskiy K.;Zosso, D. Variational Mode Decomposition. IEEE Transactions on Signal Processing, vol. 62, no. 3, pp. 531–544, 2014.
[19] Moody, G.; Mark, R.; Goldberger, A. PhysioNet: A web-based resource for the study of physiologic signals. IEEE Eng. Med. Biol. Mag. 20(3), 70–75 (2001).
[20] Bertsekas, D.P. Constrained optimization and Lagrange multiplier methods. Academic Press, New York (1982).
[21] Pan J.; Tompkins, W.J. Real-time QRS detection algorithm. IEEE Trans. Biomed. Eng., vol. 32, no. 3, pp. 230-236, March 1985.
[22] Yegnanarayana, B. Artificial Neural Networks; PHI Learning Pvt. Ltd.: New Delhi, India, 1999.
[23] Chawla, N.V.; Hall,L.O.; Bowyer, K.W.; Kegelmeyer, W.P. SMOTE: synthetic minority oversampling technique," Journal of Artificial Intelligence Research, 16:321-357, 2002.